Field-tuned chiral transport in charge-ordered CsV3Sb5

Chunyu Guo (chunyu.guo@epfl.ch)
Ecole Polytechnique Federale de Lausanne (EPFL) https://orcid.org/0000-0001-8339-7477
Carsten Putzke
Laboratory of Quantum Materials https://orcid.org/0000-0002-6205-9863
Sofia Konyzheva
EPFL
Xiangwei Huang
Ecole Polytechnique Federale de Lausanne (EPFL)
Martin Gutierrez-Amigo
CSIC-UPV/EHU
Ion Errea
University of the Basque Country https://orcid.org/0000-0002-5719-6580
Dong Chen
Max-planck institute
Maia Vergnior
Max-planck institute
Claudia Felser
Max Planck Institute for Chemical Physics of Solids https://orcid.org/0000-0002-8200-2063
Mark Fischer
UZH
Titus Neupert
University of Zurich https://orcid.org/0000-0003-0604-041X
Philip Moll
École Polytechnique Fédérale de Lausanne https://orcid.org/0000-0002-7616-5886

Physical Sciences - Article

Keywords:

Posted Date: March 18th, 2022

DOI: https://doi.org/10.21203/rs.3.rs-1463351/v1

Version of Record: A version of this preprint was published at Nature on October 12th, 2022. See the published version at https://doi.org/10.1038/s41586-022-05127-9.

Field-tuned chiral transport in charge-ordered CsV_3Sb_5

Chunyu Guo*,[1] Carsten Putzke,[1,2] Sofia Konyzheva,[1] Xiangwei Huang,[1]
Martin Gutierrez-Amigo,[3,4] Ion Errea,[3,5,6] Dong Chen,[7] Maia G. Vergniory,[5,7]
Claudia Felser,[7] Mark H. Fischer,[8] Titus Neupert†,[8] and Philip J. W. Moll‡[1]

[1]*Laboratory of Quantum Materials (QMAT), Institute of Materials (IMX), École Polytechnique Fédérale de Lausanne (EPFL), CH-1015 Lausanne, Switzerland*

[2]*Max Planck Institute for the Structure and Dynamics of Matter, 22761 Hamburg, Germany*

[3]*Centro de Física de Materiales (CSIC-UPV/EHU), 20018 Donostia-San Sebastian, Spain*

[4]*Department of Physics, University of the Basque Country (UPV/EHU), Apartado 644, 48080 Bilbao, Spain*

[5]*Donostia International Physics Center, 20018 Donostia-San Sebastian, Spain*

[6]*Fisika Aplikatua Saila, Gipuzkoako Ingeniaritza Eskola, University of the Basque Country (UPV/EHU), 20018 Donostia-San Sebastian, Spain*

[7]*Max Planck Institute for Chemical Physics of Solids, 01187 Dresden, Germany*

[8]*Department of Physics, University of Zürich, Winterthurerstrasse 190, CH-8057 Zürich, Switzerland*

(Dated: March 17, 2022)

ABSTRACT

When conductors differ from their mirror image, their chirality is reflected in the electron states and their dynamics. Conventionally, mirror symmetries are broken by the atomic structure of crystals and imprint their low symmetry onto the itinerant electron states. Unusual transport properties are a hallmark of chiral crystals, such as a non-linear electric response known as electronic magneto-chiral ansiotropy (eMChA). Here we report such a transport signature in the centro-symmetric layered Kagome metal CsV_3Sb_5, observed via second harmonic generation under magnetic field. We observe the signal in a charge-ordered phase of the material, which has been proposed to be a loop-current phase with spontaneously broken mirror symmetries. While charge ordering sets in at $T_{\mathrm{CDW}} \sim 94$ K, the eMChA transport becomes significant only at temperatures below $T' \sim 34$ K, indicative of further evolutions of this ordered phase upon lowering the temperature. Crucially, we demonstrate that the nonlinear magnetotransport can be switched by small out-of-plane fields, in accordance with recent tunneling microscopy experiments. Unlike structurally chiral materials, our results demonstrate how the electronic chirality of a metal can be tuned and even abruptly switched by small changes in magnetic fields alone – a prerequisite for their applications in chiral electronics.

INTRODUCTION

The role symmetries play in determining the properties of matter can hardly be overstated. Two opposite extremes are particularly interesting in crystalline solids: Higher symmetries constrain emergent degrees of freedom to mimic free particles — creating, for instance, massless Dirac or Weyl fermions that recover at low energies almost the full Lorentz group of free space[1–4]. This allows the observation of analogues of high-energy phenomena in table-top experiments, such as the chiral anomaly[5]. A second angle is to study systems with low symmetry, which enables novel responses that would otherwise be symmetry-forbidden. Among these, asymmetric systems characterized as *chiral* play a special role across biology, chemistry, and physics[6–8]. Crystals are structurally chiral if they possess no mirror, inversion or roto-inversion symmetry, giving rise to left-handed and right-handed versions, the so-called enantiomers. This chirality can be imprinted on the crystals' emergent excitations, which are then also characterized by a definite handedness. The interaction between structural chirality and the breaking of time-reversal symmetry (TRS) is of

particular interest, as it links the static chirality to temporal processes such as growth, catalysis, and wave propagation[9,10]. Response functions that jointly arise due to chirality and TRS breaking are called magneto-chiral anisotropies[11]. In order to isolate these response functions in measurements, it is desirable to study systems in which these symmetry properties can be controlled.

Specifically, in metals one studies the electronic magneto-chiral anisotropy (eMChA), which opens up possibilities to detect, manipulate and utilize chiral properties in electronics. It usually refers to a change in resistance R due to an applied current $\boldsymbol{I}$ and external magnetic field $\boldsymbol{B}$ that is conventionally expressed as $R(\boldsymbol{B},\boldsymbol{I}) = R_0(1+\mu^2\boldsymbol{B}^2+\gamma^{\pm}\boldsymbol{B}\cdot\boldsymbol{I})$[12], see Fig. 1. Time-reversal symmetry in non-magnetic metals enforces a magnetoresistance even in field, hence the lowest order expansion of the resistance in magnetic field is quadratic and usually takes the semi-classical form $\mu^2\boldsymbol{B}^2$ with μ the mobility. In principle, the scalar product $\boldsymbol{B}\cdot\boldsymbol{I}$ under finite applied transport current $\boldsymbol{I}$ is TRS and would allow $\boldsymbol{B}$ to enter in linear order, yet if a conductor has space-reflection symmetries this term is forced to vanish. The latter are not present in chiral crystals, and hence eMChA is allowed to appear. Its strength is described by the coupling constant $\gamma^{\pm}$ which takes opposite sign for the two enantiomers, $\gamma^{+} = -\gamma^{-}$, and is tensorial in anisotropic conductors. In effect, eMChA is a field-tuned diode-like behavior that discriminates between the polarities of the applied transport current, which is most commonly detected by the associated second-harmonic voltage generation under low-frequency AC currents.

To display eMChA, a conductor must break inversion symmetry, which can occur as a weak effect in any metal when its macroscopic shape is chiral[13–15], for example in a coil (Fig. 1). Alternatively, materials with chiral crystal structure[12,16,17] generally show eMChA that appears in any conductor shape, even simple rectangular bars or wires[18]. eMChA expresses an imbalance between scattering processes of different handedness, which can either occur from the intrinsic handedness of the carriers in chiral crystals, or extrinsically from chiral defects as in plastically twisted conductors. When electronic interactions form ordered phases within chiral materials, as for example in chiral magnets, eMChA can be further amplified via scattering off, e.g., an emergent chiral spin texture[19,20]. Importantly, in all these cases the electronic chirality follows the conductor's structural chirality, determined by the macro- or microscopic arrangement of its atoms.

In this work, we demonstrate eMChA in a rectangular bar of CsV_3Sb_5, a layered metal in which vanadium atoms form Kagome nets. In this system, a cascade of correlated symmetry-breaking electronic phases emerges at low temperatures[21–26], including a charge-density-wave (CDW) state

below $T_{\mathrm{CDW}} \approx 94$ K and superconductivity below $T_c \approx 2.5$ K[22,27–30]. These unique properties render this system an attractive platform for exploring the interplay between electronic correlations, topology and superconductivity. Crucially, this system is centro-symmetric at high temperatures, yet the relevant mirror symmetries are spontaneously broken by correlated phases of the itinerant carriers (Fig. 1). In contrast to structurally chiral crystals, which impose their chirality onto the electronic system, here a charge order breaks the mirror symmetries. As an unusual consequence, the material's chirality itself can be tuned, and even switched, as we demonstrate. The chiral character of the electronic structure within the CDW phase has been observed in scanning tunneling microscopy (STM) experiments, and its handedness was switched by an external magnetic field[31] of 2 T.

Interestingly, a second STM study[32] did not see an impact of the magnetic field on the chiral CDW. Our experiments reveal a sample dependence due to strong coupling between the CDW and subtle differences in the lattice as a likely resolution of this discrepancy, which is not surprising in CDW systems[33]. To truly obtain a symmetry lowering from spontaneous symmetry breaking, it is critical to avoid any accidental strain fields that may break the symmetry explicitly. To do so, we decouple the crystalline bar mechanically as much as possible from its supporting substrate[34] (Fig. 2a). Focused Ion Beam machining is used to gently carve c-direction aligned bars from the soft, platelet-like single crystals. The typically 10 μm long, 8 μm wide and 4 μm thick bars are structured into a 6-point geometry to either probe out-of-plane or in-plane conduction. This structure is mechanically supported by a free-standing, gold-coated SiN_x membrane (200 nm thick) which was cut into soft, meandering springs. Finite element simulations suggest that differential thermal contraction leads to strains no larger than 20 bar within the microstructure, in agreement with the sharp resistive transition at T_{CDW} and T_c observed in our structures. Indeed, any signatures of chiral transport vanish in a reference experiment with strong strain fields caused by substrate coupling, providing a natural explanation for the opposing STM experiments (see supplement).

Our main observation is the appearance of a strong second harmonic response, $V_{2\omega}$, to a low-frequency transport current (17 Hz) which distinctly evidences chiral transport within the charge-ordered state at low temperatures (Fig. 2). First, we discuss out-of-plane currents under an approximately in-plane magnetic field which is purposely misaligned by 0.5° with respect to the Kagome planes. At zero field and T = 5 K just above the superconducting transition, no second harmonic is observed, yet the signal quickly grows with increasing magnetic field. Its field-dependence is well described by $V_{2\omega} \propto B^3$ up to 18 T, the highest fields accessible to the experiment. This strikingly

departs from the behavior of structurally chiral materials such as α-Te[12], where $V_{2\omega}$ displays a linear field-dependence as described by $\Delta R/R_0 = \gamma^{\pm}\boldsymbol{B}\cdot\boldsymbol{I}$[12]. This suggests that the magnitude of eMChA itself is field dependent, given by $\gamma^{\pm}(\boldsymbol{B})$. eMChA depends on the relative direction of field and current, and hence even in a non-linear scenario, $V_{2\omega}(\boldsymbol{B})$ must change sign when the field polarity reverses, as observed experimentally. This anti-symmetric field-dependence provides strong evidence against a putative thermal origin of second harmonic voltage generation by Joule heating, as the linear magnetoresistance is even in magnetic field. Pronounced quantum oscillations are also observed above $B = 10$ T demonstrating an influence of Landau quantization on eMChA. This behavior is quantitatively consistently observed in two devices with different mechanical mounting approaches, rendering potential torque artefacts due to the soft-mounted structure unlikely. An identically shaped sample probing in-plane transport does not show second harmonic generation at any field configuration, demonstrating eMChA to be most relevant only in the interplane transport (see supplement).

To elucidate the origin of eMChA in this centro-symmetric material, we next turn to its temperature dependence. Figure 2b displays the raw $V_{2\omega}(\boldsymbol{B})$ without anti-symmetrization. Yet elevating the temperature suppresses eMChA, and at lower signal levels the weak thermal second-harmonic generation can obscure the chiral transport signatures. Hence the discussion at elevated temperatures focuses on its anti-symmetric component, $\Delta V_{2\omega} = V_{2\omega}(18\,\mathrm{T}) - V_{2\omega}(-18\,\mathrm{T})$ (see supplement for full data). At high temperatures above T_{CDW}, no $\Delta V_{2\omega}$ is observed as required for a bar-shaped crystal with centro-symmetry. The transition into the CDW state is clearly evident as a sharp spike in $\Delta V_{2\omega}$ at T_{CDW}. However, this does not reflect an eMChA response but is a result of the non-analyticity of $\rho_c(T)$ at the first-order CDW phase transition. Indeed, no anti-symmetric second harmonic signal is observed at temperatures slightly below the transition, and it only emerges at temperatures below 70 K. Its slow increase upon decreasing temperature suddenly accelerates at $T' \approx 34$ K, apparent as a change in slope on the logarithmic scale. At lower temperatures, $\Delta V_{2\omega}$ increases significantly and saturates at its maximum value below 3 K. While this only evidences the absence of chiral scattering and does not exclude a chiral order at T_{CDW} that merely does not affect transport, our results are suggestive of the onset of chiral ordering at a secondary transition at lower temperature. In particular, this temperature dependence is in correspondence with muon relaxation experiments, which detect the onset of TRS-breaking around 70 K and a subsequent rearrangement of local field distribution at 30 K[25,35,36].

The unusual nature of the eMChA in CsV_3Sb_5 becomes apparent when the field orientation is

varied with respect to the Kagome planes ($\theta = 0°$ denotes the in-plane field orientation, Fig. 3). No $V_{2\omega}$ is observed at large field angles ($\theta > 10°$). Only within a narrow angle range, $\theta = \pm 10°$, $V_{2\omega}$ quickly grows as the field-angle approaches $\theta = 0°$. It reaches a maximum around $\theta \sim 0.5°$, the configuration discussed previously in Fig. 2. For smaller θ, $V_{2\omega}$ rapidly decreases and vanishes for fields within the Kagome planes ($\theta = 0°$). Upon further rotation to small negative θ, the signal repeats yet with opposite sign. This marks a most striking aspect of the data: Tilting the field across the Kagome nets changes the handedness of the material. Rotating the field by $1°$ barely changes $\boldsymbol{B}$, hence an abrupt sign-change of $V_{2\omega}$ implies a sign-change of γ. Furthermore, its magnitude strongly reduces upon raising the temperature or lowering the field strength, while the angular extent and the sharp anomaly at the in-plane field persists. At temperatures above 35 K the peak is hardly observable, and the faint residual anomaly reflects the exponential drop of $V_{2\omega}$ above T' (Fig. 2d).

Such ease of magnetic manipulation of the electronic chirality suggests the low-temperature state differs from a simple chiral charge redistribution, as for example observed in the $3q$ chiral CDW[37] state of $TiSe_2$. Such a static charge redistribution only couples to magnetic fields via higher-order interactions, and its involved lattice response renders it unlikely to be easily manipulated at temperatures well below T_{CDW}. Instead, the experimental situation in CsV_3Sb_5 points to coupled TRS breaking, including the concomitant magnetic anomalies at T_{CDW}, the field-tunability, as well as muon spectroscopy experiments[35,36]. As a microscopic picture for this correlated state, an orbital loop current phase in the Kagome planes has been proposed that is consistent with these experimental observations[26,38,39].

In order to discuss the striking signal for fields almost in plane, we first note that unlike in previous eMChA studies, where conventional resistance remains field-independent, already the magnetoresistance of CsV_3Sb_5 displays an approximately linear in B behavior for small angles θ at high magnetic fields (see supplement), as commonly observed in semi-metals[40–42]. From the data, a phenomenological form of the resistance is $R(\boldsymbol{B}, I_z) = R_0[1 + f(\theta)|\boldsymbol{B}| + \gamma(\theta) I_z |\boldsymbol{B}|^3]$, where $f(\theta)$ and $\gamma(\theta)$ are an even and an odd function of θ, both peaked near $\theta = 0$ and I_z is the current along the crystallographic c direction. For magnetic fields and currents accessible to our experiment, we have $1 \gg \gamma(\theta) I_z |\boldsymbol{B}|^3$, so that we can think of this term as a perturbation to the resistivity, while the same is not true for $f(\theta)|\boldsymbol{B}|$, in particular for small θ. The strong θ dependence of both the eMChA coefficient γ and of the first-order resistance means that eMChA cannot be characterized by a constant tensor, as common practice in conventional eMChA materials. Yet, we can gain some

insights about the magnitude of eMChA by computing $\Delta R \,/\, (R|\boldsymbol{B}||\boldsymbol{J}|) = 4V_{2\omega} \,/\, (V_\omega|\boldsymbol{B}||\boldsymbol{J}|)$for given magnetic field strength, see Fig. 3d[12], for quantitative comparisons to other systems[43]. At B = 18 T and $\theta = 0.5°$ we find $\Delta R \,/\, (R|\boldsymbol{B}||\boldsymbol{J}|) \approx 2.4\times\ 10^{-11}$ m^2 / T·A. In comparison, this value is smaller than its record observations in t-Te[12] (10^{-8} m^2 / T·A) and TTF-ClO_4[16] (10^{-10} m^2 / T·A), where the distinct structural chirality results in relatively large eMChA, while it is larger than that of chiral magnets such as $CrNb_3S_6$[19](10^{-12} m^2 / T·A) and MnSi[20](10^{-13} m^2 / T·A), in which the chiral spin texture plays a major role in eMChA.

As the conventional eMChA analysis is only applicable for materials with negligible magnetoresistance, to further capture the field-tuned behavior of the response in CsV_3Sb_5, we next change to a description in terms of the conductance σ. For purely longitudinal transport, the conductance is the inverse of the resistance when the Hall resistivity is negligible (see supplement) such that our phenomenological form yields $\sigma = \sigma_0(\boldsymbol{B}) + \Delta\sigma(\boldsymbol{B}, \boldsymbol{I}) \approx [1 - \gamma(\theta) I_z|\boldsymbol{B}|^3] \,/\, [R_0 + R_0 f(\theta)|\boldsymbol{B}|]$. We can thus extract $\Delta\sigma \approx V_{2\omega} \,/\, V_\omega^2$, where $V_\omega = [R_0 + R_0 f(\theta)|\boldsymbol{B}|]I_z$. For field applied approximately in-plane, $\Delta\sigma$ is approximately linear in B which yields a field-independent first order derivative $\partial(\Delta\sigma)/\partial B$, see Fig. 4. The sudden sign reversal of $\partial(\Delta\sigma)/\partial B$ for small θ then suggests that the out-of-plane component of the field, B_z, has a non-perturbative effect on the system and we treat it separately, while the in-plane component is a perturbation to linear order. In other words, we write $\Delta\sigma(\boldsymbol{B}, I_z) = \tilde{\sigma}(B_z) B_x I_z$. Note that such a coupling is only allowed for a system, which breaks the $y \mapsto -y$ mirror symmetry. With $\Delta\sigma(\boldsymbol{B}, I_x)$ vanishingly small, no similar conclusion can be drawn for the mirror symmetry $z \mapsto -z$.

The behavior of $\Delta\sigma$ seen in our experiment demonstrates that the charge order in CsV_3Sb_5 (i) breaks in-plane mirror symmetries, at least below $T' \sim 34$ K and (ii) can be manipulated with an out-of plane magnetic field in the same temperature regime. We thus establish that the tunability of the chirality of charge order in CsV_3Sb_5, previously seen in STM experiments, is a macroscopic bulk property of the unconventional charge order.

We further propose the following qualitative scenario that would be consistent with our experimental observations and calls for confirmation by local-probe techniques (Fig. 4). B_z is the natural tuning parameter in Kagome net physics, as evidenced by our as well as STM experiments. Akin to a soft ferromagnet, large values of B_z (large θ) induce a fully polarized, mono-chiral state. In this polarized state, only intrinsic chiral scattering processes induce eMChA, which commonly are weak. As the field is tilted towards the plane, B_z is reduced and domains of opposite chirality appear, which act as ideal chiral scattering centers. Hence domain wall scattering may lead to ad-

ditional, extrinsic eMChA. At even smaller B_z for fields very close to the planes, both chiralities appear symmetrically and hence a globally averaging probe like transport observes a macroscopically symmetric conductor with vanishing eMChA. A fully symmetric process appears if the field is turned further, yet with inverted roles of majority and minority chirality.

Such a scenario would be compatible with the experimental observations, in particular the sharp sign change of $\tilde{\sigma}(B_z) \sim \mathrm{sign}(B_z)$ for $B_z \ll B_x$, due to a sudden flip of the majority chirality. While eMChA senses the chiral component of the scattering potential, such a domain scattering scenario inevitably would also lead to overall enhanced scattering and thereby an increase in the linear resistance. This is indeed observed, and it is interesting to note that the increase of linear magnetoresistance correlates with the emergence of eMChA. At low angles, a field-dependent $\Delta\sigma(\boldsymbol{B})$ is natural as B_z tunes the chirality. In this scenario, the chirality switching is driven by B_z independent of the in-plane field, in particular it would also occur for fully out-of-plane fields, where no eMChA is observed in our experiment. Yet unlike structurally chiral systems, here the magnetic field plays a dual role. While B_z sensitively changes the sign of $\partial(\Delta\sigma)/\partial B$, the large in-plane field is essential to observe finite eMChA, as $\Delta\sigma \propto I_z|\boldsymbol{B}|$. Naturally, a local probe like STM would observe a chiral structure, and occasionally the required domain boundaries between them, as indeed is the experimental situation[31,32].

While the small magnitude and extreme environmental conditions likely preclude direct applications, it showcases that spontaneous symmetry breaking can be utilized to transform small changes in external fields into singular changes in the response functions of chiral conductors. Hence the observation of field-switchable chiral transport further supports a picture of a highly frustrated, strongly interacting electron system on the Kagome planes of CsV_3Sb_5. Importantly, recent works have separately shown the charge-ordered state to be chiral and uncovered TRS breaking[31,35], yet our results demonstrate these two aspects to be intimately connected and thereby show a direct realization of the possible utilities that correlated electron systems hold.

[1] M. Z. Hasan and C. L. Kane, Rev. Mod. Phys. **82**, 3045 (2010).

[2] X.-L. Qi and S.-C. Zhang, Rev. Mod. Phys. **83**, 1057 (2011).

[3] N. P. Armitage, E. J. Mele, and A. Vishwanath, Rev. Mod. Phys. **90**, 015001 (2018).

[4] B. Q. Lv, T. Qian, and H. Ding, Rev. Mod. Phys. **93**, 025002 (2021).

[5] N. P. Ong and S. Liang, Nature Reviews Physics **3**, 394 (2021).

[6] J. R. Brandt, F. Salerno, and M. J. Fuchter, Nature Reviews Chemistry **1**, 0045 (2017).

[7] L. D. Barron, Israel Journal of Chemistry **61**, 517 (2021).

[8] S.-H. Yang, R. Naaman, Y. Paltiel, and S. S. P. Parkin, Nature Reviews Physics **3**, 328 (2021).

[9] S. Mühlbauer, B. Binz, F. Jonietz, C. Pfleiderer, A. Rosch, A. Neubauer, R. Georgii, and P. Böni, Science **323**, 915 (2009).

[10] K. Inoue, Chemistry Letters **50**, 742 (2021).

[11] M. Atzori, C. Train, E. A. Hillard, N. Avarvari, and G. L. Rikken, Chirality **33**, 844 (2021).

[12] G. L. J. A. Rikken and N. Avarvari, Phys. Rev. B **99**, 245153 (2019).

[13] G. L. J. A. Rikken, J. Fölling, and P. Wyder, Phys. Rev. Lett. **87**, 236602 (2001).

[14] J. Wei, M. Shimogawa, Z. Wang, I. Radu, R. Dormaier, and D. H. Cobden, Phys. Rev. Lett. **95**, 256601 (2005).

[15] V. Krstić, S. Roth, M. Burghard, K. Kern, and G. Rikken, The Journal of Chemical Physics **117**, 11315 (2002).

[16] F. Pop, P. Auban-Senzier, E. Canadell, G. L. J. A. Rikken, and N. Avarvari, Nature Communications **5**, 3757 (2014).

[17] C. Niu, G. Qiu, Y. Wang, J. Jian, H. Wang, W. Wu, and P. D. Ye, arXiv:2201.08829 (2022).

[18] We note that the "chiral electronic structure" of the symmetry-broken phase mentioned here does not necessarily have to have the symmetries of a chiral space group. In a layered, quasi-2D compound one refers to a structure as "chiral" when the in-plane mirror symmetries are broken, while the M_z mirror symmetry might still be intact. However, this lack of in-plane mirror symmetries is enough to enable the observation of eMChA in the geometry of our measurements.

[19] R. Aoki, Y. Kousaka, and Y. Togawa, Phys. Rev. Lett. **122**, 057206 (2019).

[20] T. Yokouchi, N. Kanazawa, A. Kikkawa, D. Morikawa, K. Shibata, T. Arima, Y. Taguchi, F. Kagawa, and Y. Tokura, Nature Communications **8**, 866 (2017).

[21] H. Zhao, H. Li, B. R. Ortiz, S. M. Teicher, T. Park, M. Ye, Z. Wang, L. Balents, S. D. Wilson, and I. Zeljkovic, Nature **599**, 216 (2021).

[22] Z. Liang, X. Hou, F. Zhang, W. Ma, P. Wu, Z. Zhang, F. Yu, J.-J. Ying, K. Jiang, L. Shan, Z. Wang, and X. Chen, Phys. Rev. X **11**, 031026 (2021).

[23] Y. Xiang, Q. Li, Y. Li, W. Xie, H. Yang, Z. Wang, Y. Yao, and H.-H. Wen, Nature Communications **12**, 6727 (2021).

[24] M. Kang, S. Fang, J.-K. Kim, B. R. Ortiz, S. H. Ryu, J. Kim, J. Yoo, G. Sangiovanni, D. Di Sante, B.-G. Park, C. Jozwiak, A. Bostwick, E. Rotenberg, E. Kaxiras, S. D. Wilson, J.-H. Park, and R. Comin, Nature Physics (2022).

[25] L. Nie, K. Sun, W. Ma, D. Song, L. Zheng, Z. Liang, P. Wu, F. Yu, J. Li, M. Shan, D. Zhao, S. Li, B. Kang, Z. Wu, Y. Zhou, K. Liu, Z. Xiang, J. Ying, Z. Wang, T. Wu, and X. Chen, Nature (2022).

[26] M. M. Denner, R. Thomale, and T. Neupert, Phys. Rev. Lett. **127**, 217601 (2021).

[27] B. R. Ortiz, L. C. Gomes, J. R. Morey, M. Winiarski, M. Bordelon, J. S. Mangum, I. W. Oswald, J. A. Rodriguez-Rivera, J. R. Neilson, S. D. Wilson, E. Ertekin, T. M. McQueen, and E. S. Toberer, Phys. Rev. Mater. **3**, 094407 (2019).

[28] B. R. Ortiz, S. M. Teicher, Y. Hu, J. L. Zuo, P. M. Sarte, E. C. Schueller, A. M. Abeykoon, M. J. Krogstad, S. Rosenkranz, R. Osborn, R. Seshadri, L. Balents, J. He, and S. D. Wilson, Phys. Rev. Lett. **125**, 247002 (2020).

[29] F. Yu, T. Wu, Z. Wang, B. Lei, W. Zhuo, J. Ying, and X. Chen, Phys. Rev. B **104**, L041103 (2021).

[30] C. Mu, Q. Yin, Z. Tu, C. Gong, H. Lei, Z. Li, and J. Luo, Chin. Phys. Lett. **38**, 077402 (2021).

[31] Y.-X. Jiang, J.-X. Yin, M. M. Denner, N. Shumiya, B. R. Ortiz, G. Xu, Z. Guguchia, J. He, M. S. Hossain, X. Liu, J. Ruff, L. Kautzsch, S. S. Zhang, G. Chang, I. Belopolski, Q. Zhang, T. A. Cochran, D. Multer, M. Litskevich, Z.-J. Cheng, X. P. Yang, Z. Wang, R. Thomale, T. Neupert, S. D. Wilson, and M. Z. Hasan, Nature Materials **20**, 1353 (2021).

[32] H. Li, H. Zhao, B. R. Ortiz, T. Park, M. Ye, L. Balents, Z. Wang, S. D. Wilson, and I. Zeljkovic, Nature Physics , 1 (2022).

[33] G. Grüner, Rev. Mod. Phys. **60**, 1129 (1988).

[34] X. Huang, C. Guo, C. Putzke, Y. Sun, M. G. Vergniory, I. Errea, M. Gutierrez, D. Chen, C. Felser, and P. J. W. Moll, arXiv:2201.07780 (2022).

[35] C. Mielke, D. Das, J.-X. Yin, H. Liu, R. Gupta, Y.-X. Jiang, M. Medarde, X. Wu, H. C. Lei, J. Chang, P. Dai, Q. Si, H. Miao, R. Thomale, T. Neupert, Y. Shi, R. Khasanov, M. Z. Hasan, H. Luetkens, and Z. Guguchia, Nature **602**, 245 (2022).

[36] L. Yu, C. Wang, Y. Zhang, M. Sander, S. Ni, Z. Lu, S. Ma, Z. Wang, Z. Zhao, H. Chen, K. Jiang, Y. Zhang, H. Yang, F. Zhou, X. Dong, S. L. Johnson, M. J. Graf, J. Hu, H.-J. Gao, and Z. Zhao, arXiv:2107.10714 (2021).

[37] J. Ishioka, Y. H. Liu, K. Shimatake, T. Kurosawa, K. Ichimura, Y. Toda, M. Oda, and S. Tanda, Phys. Rev. Lett. **105**, 176401 (2010).

[38] X. Feng, K. Jiang, Z. Wang, and J. Hu, Science Bulletin **66**, 1384 (2021).

[39] Y.-P. Lin and R. M. Nandkishore, Phys. Rev. B **104**, 045122 (2021).

[40] C.-L. Zhang, S.-Y. Xu, I. Belopolski, Z. Yuan, Z. Lin, B. Tong, G. Bian, N. Alidoust, C.-C. Lee, S.-M. Huang, T.-R. Chang, G. Chang, C.-H. Hsu, H.-T. Jeng, M. Neupane, D. S. Sanchez, H. Zheng, J. Wang, H. Lin, C. Zhang, H.-Z. Lu, S.-Q. Shen, T. Neupert, M. Zahid Hasan, and S. Jia, Nature Communications **7**, 10735 (2016).

[41] T. Liang, Q. Gibson, M. N. Ali, M. Liu, R. J. Cava, and N. P. Ong, Nature Materials **14**, 280 (2015).

[42] J. Xiong, S. K. Kushwaha, T. Liang, J. W. Krizan, M. Hirschberger, W. Wang, R. J. Cava, and N. P. Ong, Science **350**, 413 (2015).

[43] The quantity $\Delta R \,/\, (R|\boldsymbol{B}||\boldsymbol{J}|)$ equals the constant γ when it is a field-independent parameter in chiral materials commonly used in literature.

Acknowledgements

Funding: This work was funded by the European Research Council (ERC) under the European Union's Horizon 2020 research and innovation programme (MiTopMat - grant agreement No. 715730). This project received funding by the Swiss National Science Foundation (Grants No. PP00P2_176789). M.G.V., I. E. and M.G.A. acknowledge the Spanish Ministerio de Ciencia e Innovacion (grant PID2019-109905GB-C21). M.G.V. thanks support to Programa Red Guipuzcoana de Ciencia Tecnología e Innovación 2021 No. 2021-CIEN-000070-01 Gipuzkoa Next and the Deutsche Forschungsgemeinschaft (DFG, German Research Foundation) GA 3314/1-1 – FOR 5249 (QUAST). This work has been supported in part by Basque Government grant IT979-16. This work was also supported by the European Research Council Advanced Grant (No. 742068) "TOPMAT", the Deutsche Forschungsgemeinschaft (Project-ID No. 258499086) "SFB 1143", and the DFG through the Würzburg-Dresden Cluster of Excellence on Complexity and Topology in Quantum Matter ct.qmat (EXC 2147, Project-ID No. 39085490).

Competing Interests The authors declare that they have no competing financial interests.

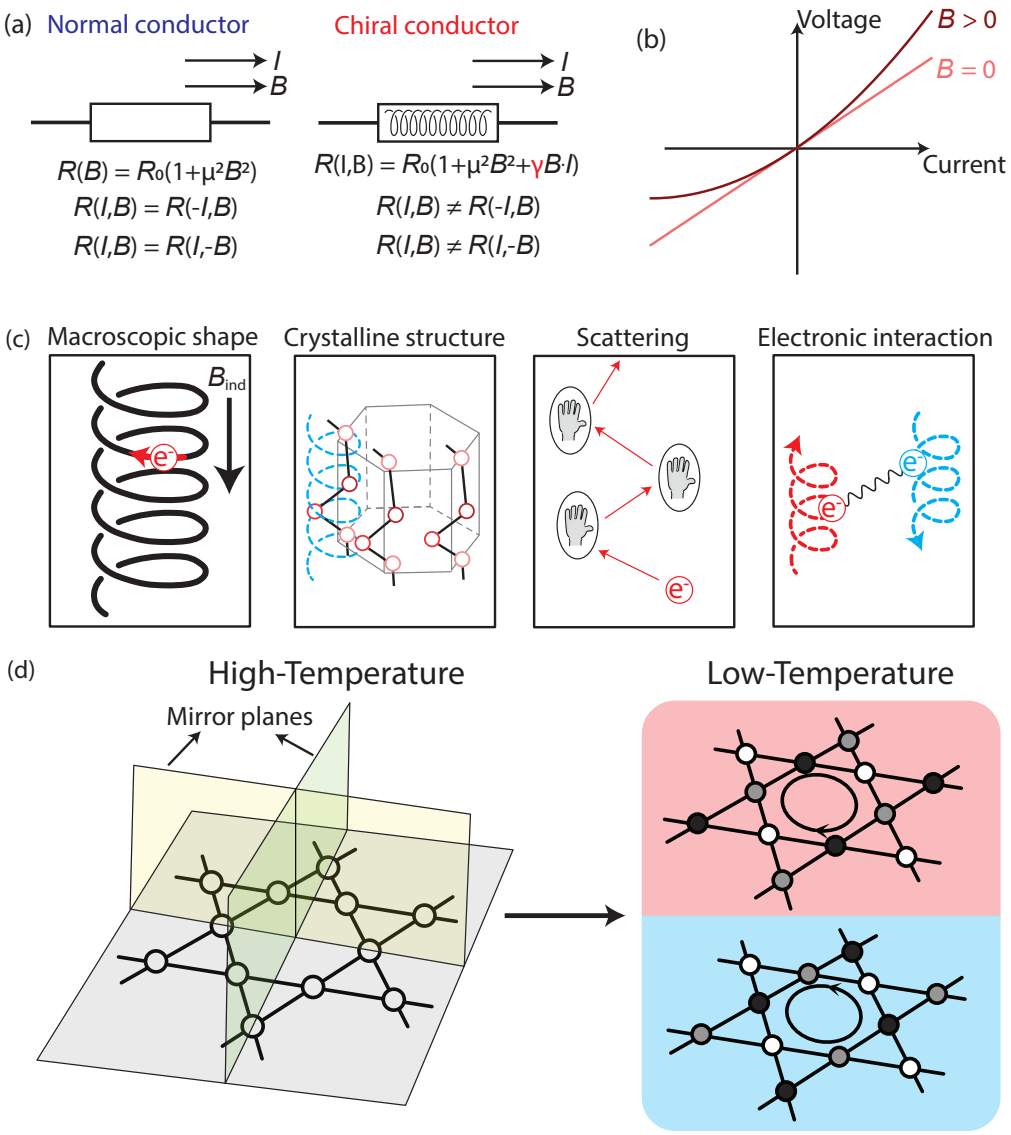

FIG. 1. (a) Illustration of electrical resistance of normal and chiral conductors within the low-frequency quasi-DC limit. (b) I(V) curve for a chiral conductor. (c) Different mechanisms for electronic magneto-chiral anisotropy. The blue dashed line in crystalline structure case represents the notation of chiral atomic chain. For the case of scattering the encircled hands represent the scattering centers with particular chirality. (d) The crystal structure of CsV_3Sb_5 preserves all mirror symmetries at high temperatures and only spontaneous symmetry breaking at low temperatures allow for a finite eMChA in a symmetric microstructure.

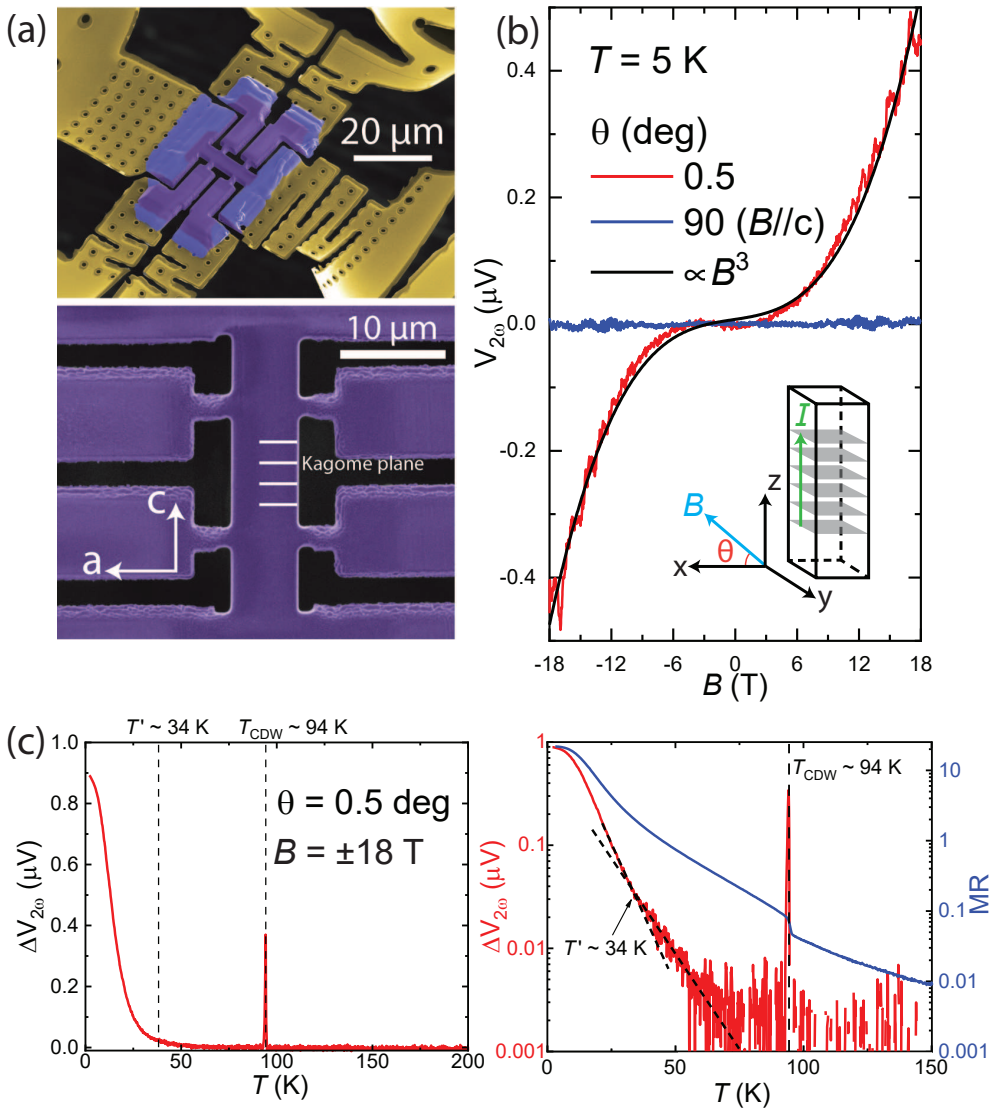

FIG. 2. (a) Low-strain microstructure fabricated by FIB. (b) Field dependence of Second harmonic voltage with current applied along z(c)-axis. The signal becomes significant when magnetic field is applied approximately along the x-axis. The inset sketches the transport bar. (c) Left hand panel displays temperature dependence of $\Delta V_{2\omega} = V_{2\omega}(18\,\mathrm{T}) - V_{2\omega}(-18\,\mathrm{T})$ with magnetic field applied approximately along x-axis. The right hand panel presents log-scale temperature dependence of $\Delta V_{2\omega}$ and magnetoresistance ratio MR = (ρ_c(18 T)-ρ_c(0))/ρ_c(0)

.

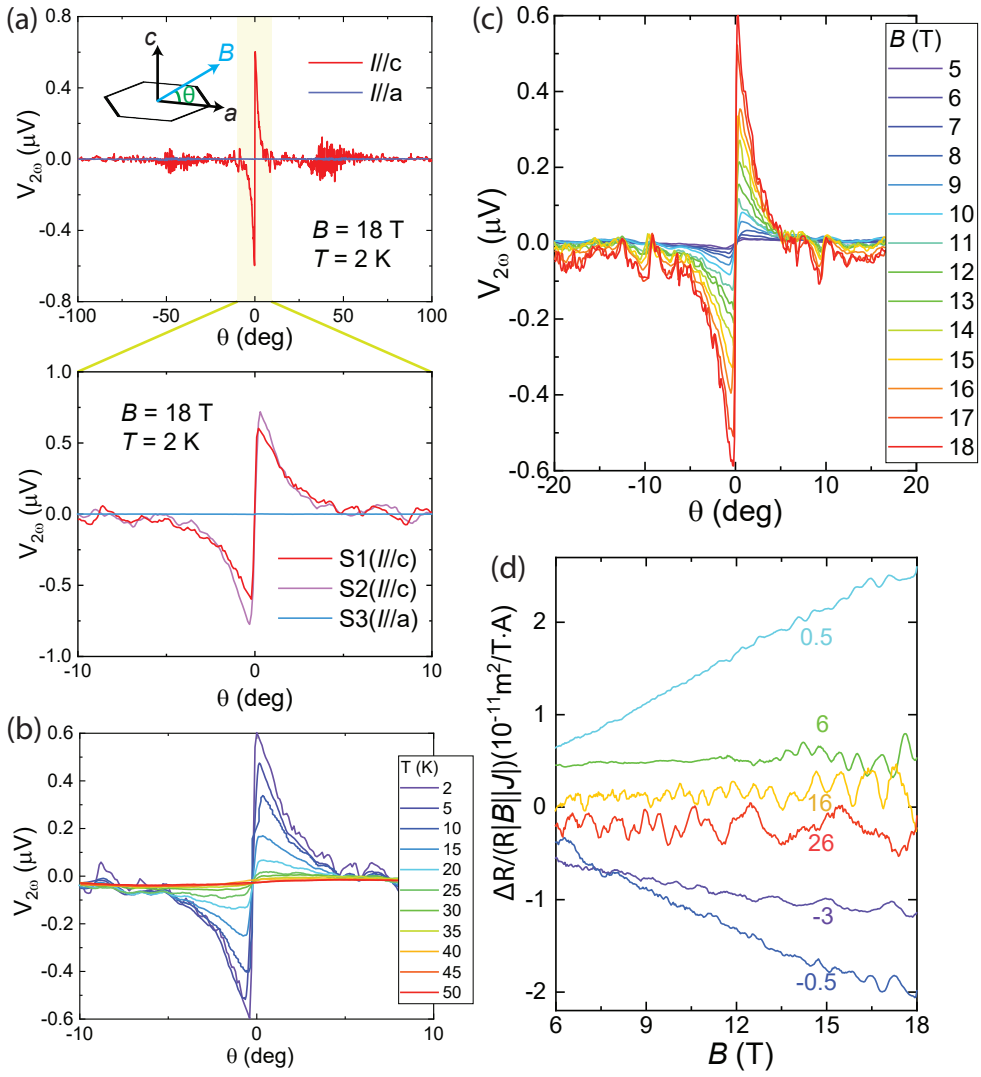

FIG. 3. (a) Angular dependence of $V_{2\omega}$ for I||a and I||c. A sharp spike with disrupt sign-reversal is observed for I||c around a-axis. Zoom-in view of small angle regime reveals the sharpness of the sign reversal which is within 0.5 degree. (b) Angular dependence of γ-coefficients at various temperatures with B = 18 T. (c) Angular dependence of γ-coefficients for various magnetic fields at T = 2 K. (d) Field-dependent eMChA-coefficients at various angles.

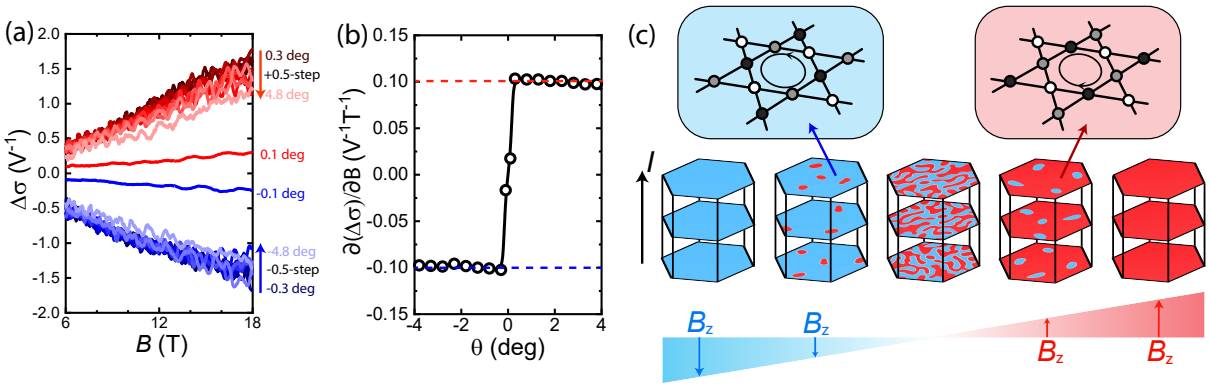

FIG. 4. (a) Field-dependence of chiral-conductivity $\Delta\sigma$ at various angles. (b) Angular dependence of the first order derivative $\partial(\Delta\sigma)/\partial B$ from B = 6 to 18 T. (c) Sketch of a chirality reversal at in-plane aligned magnetic fields. The emergence of opposite domains can naturally lead to a strong enhancement of eMChA at low field angles.

Supplementary materials for "Field-tuned chiral transport in charge-ordered CsV_3Sb_5"

Chunyu Guo*,[1] Carsten Putzke,[1,2] Sofia Konyzheva,[1] Xiangwei Huang,[1]
Martin Gutierrez-Amigo,[3,4] Ion Errea,[3,5,6] Dong Chen,[7] Maia G. Vergniory,[5,7]
Claudia Felser,[7] Mark H. Fischer,[8] Titus Neupert†,[8] and Philip J. W. Moll‡[1]

[1]*Laboratory of Quantum Materials (QMAT), Institute of Materials (IMX), École Polytechnique Fédérale de Lausanne (EPFL), CH-1015 Lausanne, Switzerland*

[2]*Max Planck Institute for the Structure and Dynamics of Matter, 22761 Hamburg, Germany*

[3]*Centro de Física de Materiales (CSIC-UPV/EHU), 20018 Donostia-San Sebastian, Spain*

[4]*Department of Physics, University of the Basque Country (UPV/EHU), Apartado 644, 48080 Bilbao, Spain*

[5]*Donostia International Physics Center, 20018 Donostia-San Sebastian, Spain*

[6]*Fisika Aplikatua Saila, Gipuzkoako Ingeniaritza Eskola, University of the Basque Country (UPV/EHU), 20018 Donostia-San Sebastian, Spain*

[7]*Max Planck Institute for Chemical Physics of Solids, 01187 Dresden, Germany*

[8]*Department of Physics, University of Zürich, Winterthurerstrasse 190, CH-8057 Zürich, Switzerland*

I. CRYSTAL SYNTHESIS AND CHARACTERIZATION

CsV_3Sb_5 crystallizes a P6/mmm space group which features a layered structure of Kagome planes formed by the V-atoms (Fig. S1). The single crystals were grown by the self-flux method[1]. Hexagonal plate-shaped crystals with typical dimensions of $2 \times 2 \times 0.04$ mm^3 were obtained. The crystals were characterized by the x-ray diffraction (XRD) off the maximum surface on a PANalytical diffractometer with Cu Kα radiation at room temperature. As shown in Fig. S1, all the peaks in the XRD pattern can be identified as the $(00l)$ reflections of CsV_3Sb_5.

Based on the crystalline structure we have calculated the band structure of CsV_3Sb_5 by density functional theory (DFT) using the Quantum Espresso package (QE)[2], the details of which can be found in Ref. 3[3]. The obtained electronic structure features multiple Dirac nodal lines lifted by spin-orbit coupling (SOC), leaving only symmetry-protected Dirac nodes at L-points. These results are consistent with the previous reports[1,4].

Magnetoresistivity measurements were performed with electric current and magentic field applied along out-of-plane (z) and in-plane(x) directions respectively. The magnetoresistance displays a quasi-linear field-dependence up to B = 18 T while Hall resistivity is almost negligible compared to that. This is expected as the electrical current is applied along the out-of-plane direction, Hall resistivity should vanish for such a quasi-2D material with the Brillouin zone dominated by the large cylindrical Fermi surfaces.

II. REPRODUCIBILITY OF EMCHA WITH TWO DIFFERENT DEVICES.

To show the reproducibility of the second harmonic voltage generation due to eMChA, we have measured two membrane-based devices with different mounting techniques/geometries. For device S1, the sample is completely suspended by soft Au-coated membrane springs. In comparison, device S2 is attached to the membrane only on one side, the other side of the sample is welded directly to the Si-substrate by FIB-assisted Pt-deposition. Device S2 displays a slightly broader CDW transition than S1 in the temperature dependence of resistivity across T_{CDW} yet the transition temperatures are exactly the same. This suggests a marginally larger strain gradient across the device due to thermal contraction for device S2 which is compatible with the estimated strain value presented in Sec. III. Since the strain in both devices is negligible, the second harmonic voltage is consistently observed among the two devices with similar value as well as almost identical angular

spectrum. These results demonstrate the clear consistency among different low-strain samples and therefore evidence that the observed eMChA in CsV_3Sb_5 is an intrinsic material property.

III. ESTIMATION OF STRAIN DUE TO DIFFERENTIAL THERMAL CONTRACTION

To obtain the tensile strain applied to the sample, we need to firstly estimate the total displacement due to different thermal contraction coefficients of samples and substrates used. Upon cooling from 300 K to 4 K, the integrated thermal contraction coefficient of SiN_x(ε_{SiN}) and Si(ε_{Si}) are 0.0342% and 0.0208% respectively. For the sample itself we assume a typical thermal contraction coefficient for alkali metal $\varepsilon_{Samp} \approx 0.1\%$, which provides a conservative, upper bound. Based on these parameters and the actual device geometry illustrated in Fig. S3, the total displacement can be easily obtained as:

$$dL_{S1} = L_{S1} \times \varepsilon_{Samp} = 30\ nm \tag{S1}$$

$$dL_{SiNx} = L_{SiNx} \times \varepsilon_{SiNx} = 75\ nm \tag{S2}$$

$$dL_{Si} = L_{Si} \times \varepsilon_{Si} = 52\ nm \tag{S3}$$

$$dL_{S1} = dL_{S1} + dL_{SiNx} - dL_{Si} = 53\ nm \tag{S4}$$

The spring constant of the SiN_x spring for device S1 is estimated as 125 N/m from finite element simulations (COMSOL), the total pressure can be calculated as:

$$P_{S1} = k_{S1} \cdot dL_{S1}/A = 8.8\ bar \tag{S5}$$

where A stands for the cross section of the spring.

Meanwhile for device S2, the pressure can be calculated with the same process:

$$P_{S2} = k_{S2} \cdot dL_{S2}/A = 18.7\ bar \tag{S6}$$

In both cases the pressure is less than 20 bar, which quantifies the low-strain nature of these devices.

IV. STRAIN EFFECT ON EMCHA

The necessity of low-strain mounting is revealed by a comparative study of device S4 which features a sample that is glued down to a sapphire substrate. Here the device is structured into

an "L"-shape with two long beams along both a and c-direction (Fig. S4). Since the sample and substrate are mechanically coupled via the glue droplet, the thermal contraction difference between them results in a tensile strain along the beam direction. This tensile strain shifts the CDW transition of device S4 to a higher temperature compared to the strain-free S1. Most importantly, no meaningful second harmonic voltage has been observed for device S4. These observations suggest the importance of c-axis tensile strain which restricts the sample into a mono-domain criteria and therefore completely suppressed eMChA which relies on the chiral electronic scatterings caused by domains with different chiralities. This observation suggests that residual strain fields would provide a natural explanation for the contradictory Scanning tunneling microscope(STM) experimental results[5,6].

V. FIELD-SYMMETRY ANALYSIS OF SECOND HARMONIC VOLTAGE

To further demonstrate the origin of second harmonic voltage generation, we also measured the temperature-dependent $V_{2\omega}$ at B = 18 and -18 T respectively (Fig. S5). By taking the sum and difference of these two results we obtained both the field-symmetric and asymmetric components of $V_{2\omega}$. It is clear that the asymmetric component due to eMChA dominates the total signal, while the symmetric component most likely due to Joule heating effect at the electric contacts is merely a minor part.

---

[1] B. R. Ortiz, S. M. Teicher, Y. Hu, J. L. Zuo, P. M. Sarte, E. C. Schueller, A. M. Abeykoon, M. J. Krogstad, S. Rosenkranz, R. Osborn, R. Seshadri, L. Balents, J. He, and S. D. Wilson, Phys. Rev. Lett. **125**, 247002 (2020).

[2] P. Giannozzi, O. Andreussi, T. Brumme, O. Bunau, M. B. Nardelli, M. Calandra, R. Car, C. Cavazzoni, D. Ceresoli, M. Cococcioni, N. Colonna, I. Carnimeo, A. D. Corso, S. de Gironcoli, P. Delugas, R. A. D. Jr, A. Ferretti, A. Floris, G. Fratesi, G. Fugallo, R. Gebauer, U. Gerstmann, F. Giustino, T. Gorni, J. Jia, M. Kawamura, H.-Y. Ko, A. Kokalj, E. Küçükbenli, M. Lazzeri, M. Marsili, N. Marzari, F. Mauri, N. L. Nguyen, H.-V. Nguyen, A. O. de-la Roza, L. Paulatto, S. Poncé, D. Rocca, R. Sabatini, B. Santra, M. Schlipf, A. P. Seitsonen, A. Smogunov, I. Timrov, T. Thonhauser, P. Umari, N. Vast, X. Wu, and S. Baroni, J. Phys. Condens. Mat. **29**, 465901 (2017).

[3] X. Huang, C. Guo, C. Putzke, Y. Sun, M. G. Vergniory, I. Errea, M. Gutierrez, D. Chen, C. Felser, and P. J. W. Moll, arXiv:2201.07780 (2022).

[4] B. R. Ortiz, L. C. Gomes, J. R. Morey, M. Winiarski, M. Bordelon, J. S. Mangum, I. W. Oswald, J. A. Rodriguez-Rivera, J. R. Neilson, S. D. Wilson, E. Ertekin, T. M. McQueen, and E. S. Toberer, Phys. Rev. Mater. **3**, 094407 (2019).

[5] Y.-X. Jiang, J.-X. Yin, M. M. Denner, N. Shumiya, B. R. Ortiz, G. Xu, Z. Guguchia, J. He, M. S. Hossain, X. Liu, J. Ruff, L. Kautzsch, S. S. Zhang, G. Chang, I. Belopolski, Q. Zhang, T. A. Cochran, D. Multer, M. Litskevich, Z.-J. Cheng, X. P. Yang, Z. Wang, R. Thomale, T. Neupert, S. D. Wilson, and M. Z. Hasan, Nature Materials **20**, 1353 (2021).

[6] H. Li, H. Zhao, B. R. Ortiz, T. Park, M. Ye, L. Balents, Z. Wang, S. D. Wilson, and I. Zeljkovic, Nature Physics , 1 (2022).

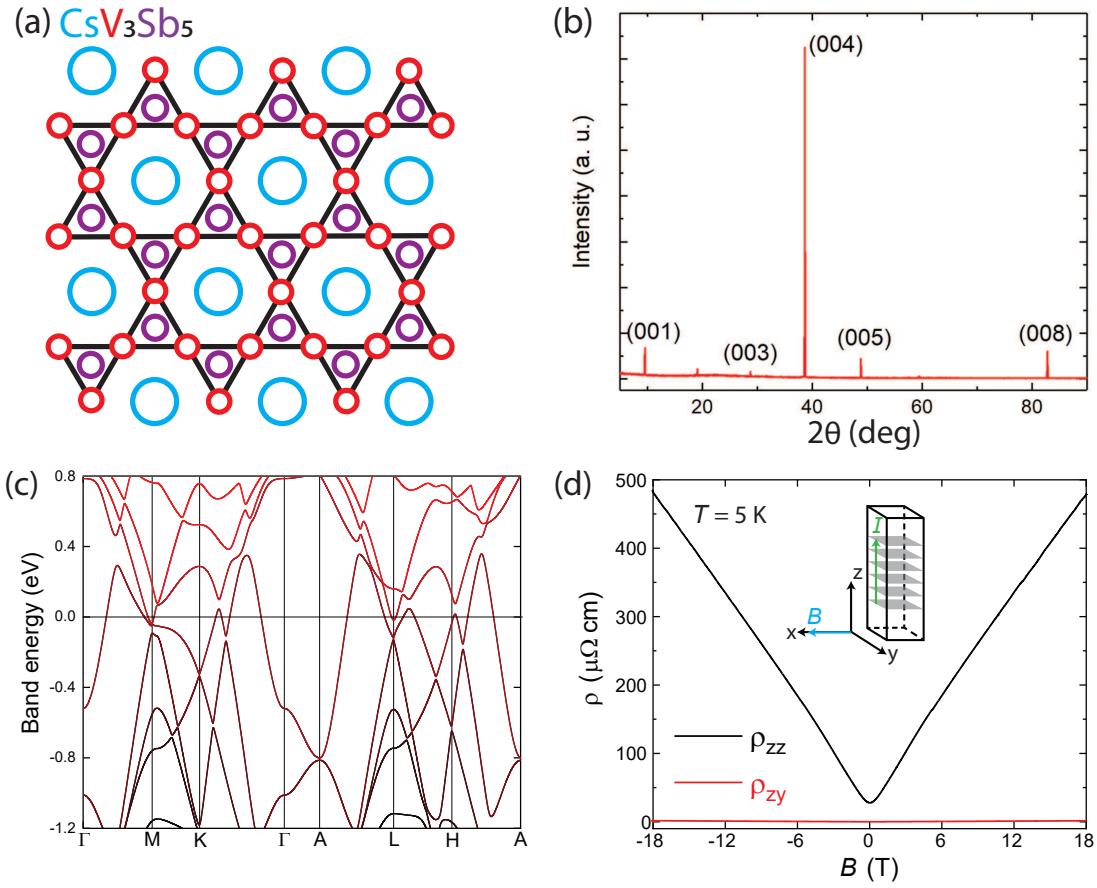

FIG. S1. (a) Crystal structure of CsV_3Sb_5. (b) XRD pattern of the (001) facet of a CsV3Sb5 crystal. (c) Band structure of CsV_3Sb_5 calculated by density functional theory (DFT) using the Quantum Espresso package (QE)[2]. (d) Field dependence of Magnetoresistivity and Hall resistivity measured at T = 5 K. A large quasi-linear magnetoresistance is observed up to B = 18 T. In comparison Hall resistivity is almost negligible.

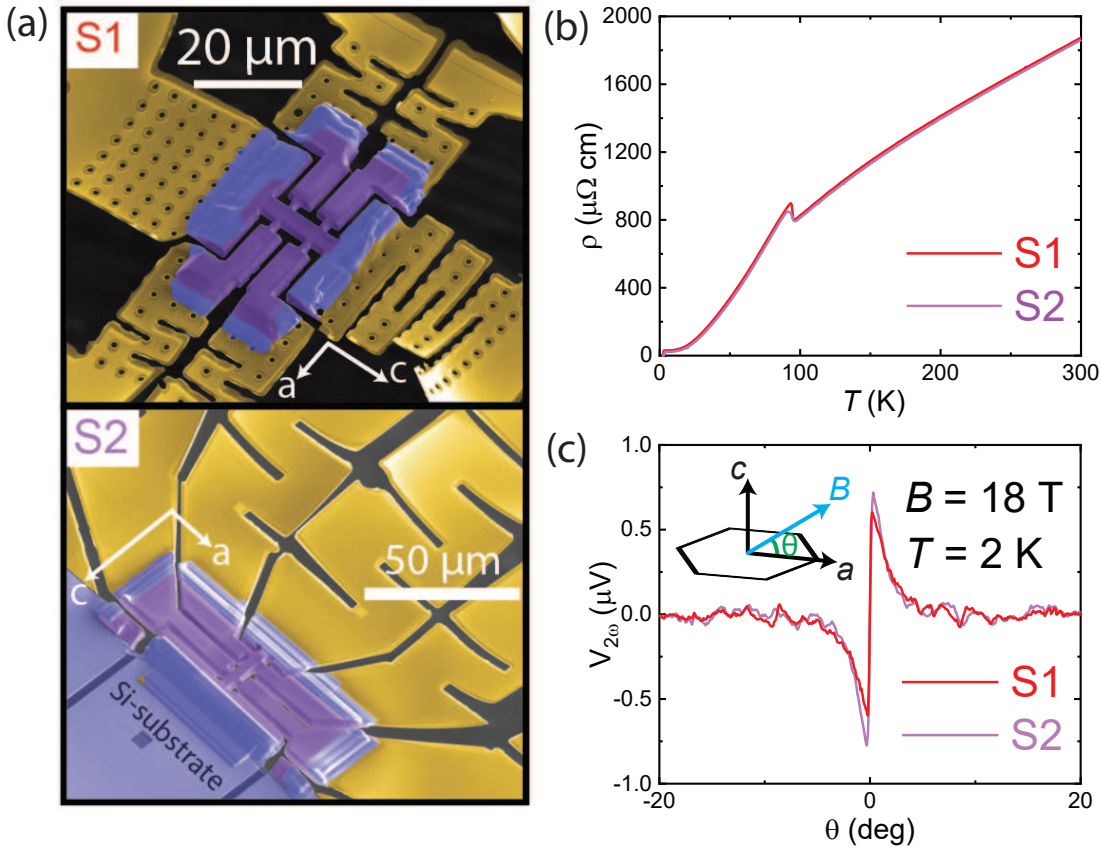

FIG. S2. (a) Scanning electron microscope(SEM) images of both device S1 and S2. (b) Temperature-dependent resistivity of S1 and S2 from 300 K to 1.6 K. (c) Angle-dependent second harmonic voltage measured at B = 18 T and T = 2 K.

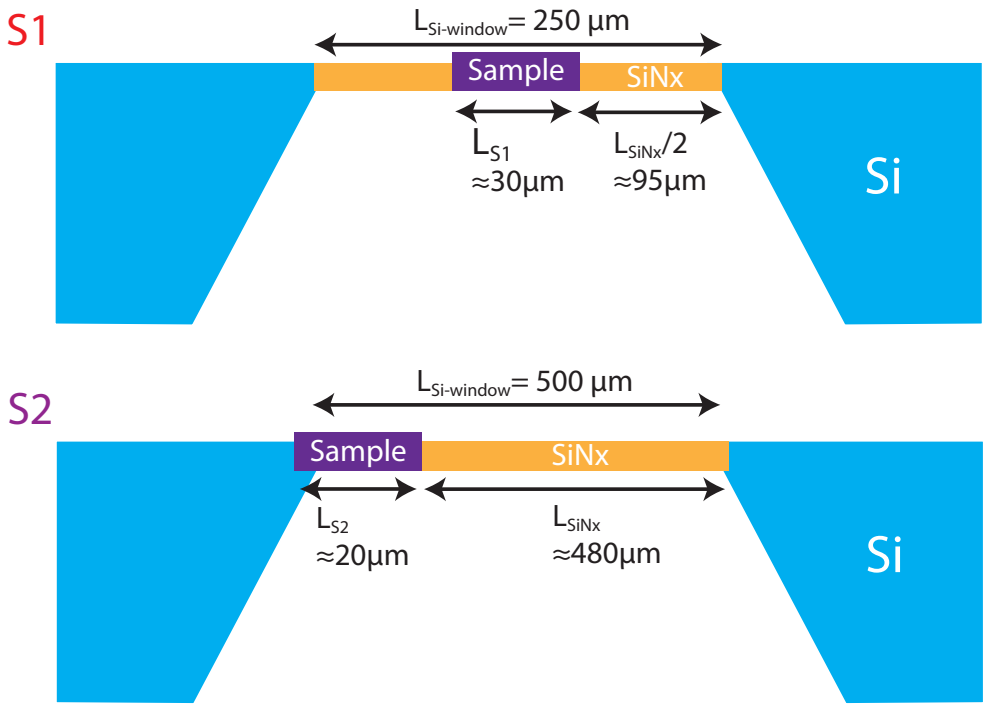

FIG. S3. Illustration of device configuration for both S1 and S2. While S1 is completely suspended by the membrane springs, S2 is attached to the Si-substrate frame on one side and membrane springs on the other side.

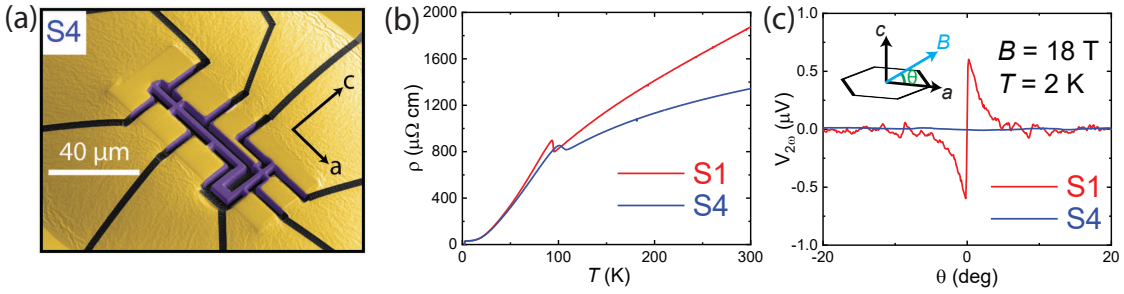

FIG. S4. (a) SEM image of device S4. The sample is attached to the sapphire substrate via a glue droplet. The thin beam along c-axis allows us to measure the electric response with both current and tensile strain applied along c-axis. (b) Temperature dependence of resistivity for S1 and S4. The CDW transition is enhanced to a higher temperature with tensile strain along c-axis(S4). (c)Angular spectrum of second harmonic voltage ($V_{2\omega}$). Clearly $V_{2\omega}$ is completely suppressed with tensile strain along c-axis .

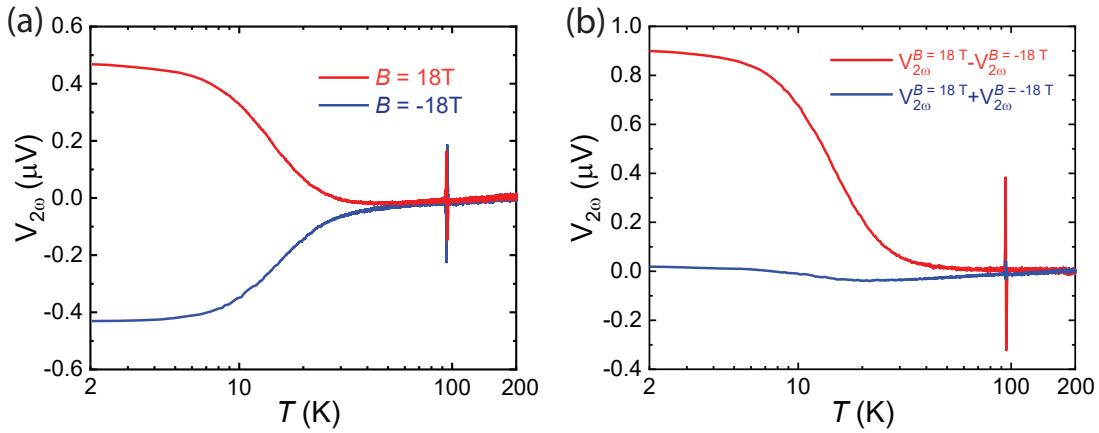

FIG. S5. (a) Temperature dependence of $V_{2\omega}$ measured at $B = \pm$ 18 T respectively. (b) Temperature-dependent field-symmetric and asymmetric part of $V_{2\omega}$.

Supplementary Files

This is a list of supplementary files associated with this preprint. Click to download.

- CsV3Sb5eMChASI.pdf